Enhanced Performance and Conversion Pathway for Catalytic Ozonation of Methyl Mercaptan on Single-Atom Ag Deposited Three-Dimensional Ordered Mesoporous MnO_2

Dehua Xia [a, b,], Wenjun Xu [a, e,], Yunchen Wang [a], Jingling Yang [a], Yajing Huang [a], Lingling Hu [a], Chun He [a, b, *], Dong Shu [c], Dennis Y.C. Leung [d,**], Zhihua Pang [e]

[a] School of Environmental Science and Engineering, Sun Yat-sen University, Guangzhou, 510275, China

[b] Guangdong Provincial Key Laboratory of Environmental Pollution Control and Remediation Technology, Guangzhou, 510275, China

[c] Key Lab of Technology on Electrochemical Energy Storage and Power Generation in Guangdong Universities, School of Chemistry and Environment, South China Normal University, Guangzhou, 510006, China

[d] Department of Mechanical Engineering, The University of Hong Kong, Pokfulam Road, Hong Kong

[e] South China Institute of Environmental Science, Ministry of Environmental Protection (MEP), Guangzhou 510655, PR China

(26 Pages including supplementary 8 Texts, 5 Table and 9 Figures)

*Corresponding author: School of Environmental Science and Engineering, Sun Yat-sen University, Guangzhou, 510275, China. Email address: hechun@mail.sysu.edu.cn (C. He); ycleung@hku.hk (D.Y.C. Leung).

Figure S8. (a) IC analysis of final catalytic products of CH_3SH using Ag/MnO_2 HPMSs; (b) FT-IR spectra of Ag/MnO_2 PHMSs after reaction and regeneration.

Figure S9. O_3 decomposition by MnO_2 and Ag/MnO_2 PHMSs.

Text S1. Materials and Synthesis of MnO_2 PHMSs.

The chemical reagents for synthesizing Ag/MnO_2 PHMSs were analytical grade and used without any further purification. $Mn(CH_3COO)_2{\cdot}4H_2O$, $AgNO_3$, Na_2CO_3, $KMnO_4$ and HCl were purchased from Tianjing Yongda Chemical Reagent Co. Ltd., Shanghai Boda Chemical Industry Co. Ltd., Shantou Xilong Chemical Industry Co. Ltd., Tianjing Fuchen Chemical Reagent Co. Ltd. and Guangzhou Reagent Chemical Industry Co. Ltd., respectively. CH_3SH gas source with a traceable concentration of 2000 ppm in N_2 was obtained from Foshan Kedi Chemical Industry Co. Ltd. Deionized water was used throughout this study.

As shown in Figure S1, Firstly, 0.01 mol $Mn(CH_3COO)_2{\cdot}4H_2O$ and 0.015 mol Na_2CO_3 were added to form white precipitates ($MnCO_3$). Secondly, the resultant $MnCO_3$ was transferred into 0.0002 M $KMnO_4$ solution to form MnO_2 shell with stirring for 4 min. Thirdly, the remaining $MnCO_3$ was removed by 0.01 M HCl. Finally, MnO_2 PHMSs were obtained by calcination in a furnace at 400 °C for 4 h.

Text S2. Characterization of Ag/MnO_2 PHMSs

The X-ray diffraction (XRD) patterns of the catalysts were collected using a Rigaku D/max 2200PC diffractometer with Cu Kα radiation. Raman spectra was obtained using a Laser Micro-Raman Spectrometer (Renishaw inVia, British) with a 514.5 nm laser source. The morphology of the catalysts was taken by JEM 2100F and H-7650 Transmission electronic microscopy (TEM) at both bright and dark fields. The images of spherical aberration-corrected high angle angular dark field scanning transmission electron microscopy (Cs-corrected HAADF-STEM) were taken from a JEM ARM 200F instrument. The chemical compositions of the catalysts were determined by X-ray photoelectron spectroscopy (XPS, ESCALAB 250, Thermo Fisher Scientific, USA). The specific surface area (BET) was determined with an ASAP2010 adsorption instrument (USA). Hydrogen temperature-programmed reduction (H_2-TPR) was performed on the BELCAT-B (Japan) instrument. Fourier transform infrared spectrometer (FT-IR) patterns were collected using an EQUIMNO2X 55 FTIR spectrometer with 0.2 cm^{-1} resolution. The resultant products were analyzed by an ion chromatography (IC, 882 Compact IC plus-Anion, Switzerland). *In situ* diffused Fourier transform infrared spectroscopy (*in situ* DRIFTS) was recorded in Thermo Fisher 6700. The mass fraction of Ag in the Ag/MnO_2 PHMSs was determined by an Inductively Coupled Plasma Optical Emission Spectrometer (ICP-OES).

The degradation efficiency of CH_3SH was calculated as follow, in which $[CH_3SH]_{in}$ and $[CH_3SH]_{out}$ represent the concentration of CH_3SH in the inlet steam and outlet stream, respectively.

$$CH_3SH \text{ degradation } (\%) = \left(1 - \frac{[CH_3SH]_{out}}{[CH_3SH]_{in}}\right) \times 100\%$$

92 **Text S3.** CV curves

93 To investigate the interaction of Ag and MnO_2 on the electron transfer progress and
94 the redox ability, the CV curves of MnO_2 and Ag/MnO_2 PHMSs are studied in a 0.1 M
95 Na_2SO_4 solution at water-catalyst interface with ozone purging and shown in Figure 1d.
96 The measurements were conducted in a conventional H-type electrochemical Pyrex cell
97 with a standard three-electrode assembly. This assembly had a MnO_2 or Ag/MnO_2
98 PHMSs working electrode, a Pt wire as a counter electrode (area, 0.5 × 1.0 cm^2), and a
99 saturated calomel electrode (SCE) as a reference electrode. To prepare MnO_2 electrodes
100 and Ag/MnO_2 PHMSs electrodes, the MnO_2 or Ag/MnO_2 PHMSs slurry were prepared
101 by dispersing 20.0 mg catalysts into 5 mL water containing 3 wt.% poly(vinyl alcohol)
102 (PVA). ITO (sheet resistance ≈ 20 Ω cm^{-2}) was employed as the substrate of MnO_2 or
103 Ag/MnO_2 PHMSs electrode.

104 The electron transfer progress and the redox ability between Ag and MnO_2 are
105 important for heterogeneous catalytic ozonation [46]. To investigate the interaction of Ag
106 and MnO_2 on the electron transfer progress and the redox ability, the CV curves of
107 Ag/MnO_2 PHMSs are studied in a 0.1 M Na_2SO_4 solution at water-catalyst interface with
108 ozone purging and shown in Figure 1d. After Ag deposition, the current of Ag/MnO_2
109 PHMSs are much higher than that of MnO_2 PHMSs, verifying the presence of higher
110 surface charge on Ag/MnO_2 PHMSs than MnO_2 PHMSs. Moreover, in the presence of
111 ozone, it is obvious to observe that current intensity of both curves was increased and the
112 peak potential shifted positive, suggesting a possible reduction process occurred on the

surface of catalysts with the decomposition of ozone. Similarly, the reduction current in case of Ag/MnO_2 PHMSs was significantly increased as compared to MnO_2 PHMSs, confirming that the Ag/MnO_2 PHMSs exhibit a favorable performance for interfacial electron transfer than MnO_2 PHMSs [47].

Text S4. Conclusion of characterization

Based on the above structural analysis, it is expected that Ag/MnO_2 PHMSs with higher density of oxygen vacancy, crystalline defect and O_L would demonstrate a better catalytic ability than MnO_2 PHMSs. In other words, the crystalline defects and oxygen vacancies provide places for the decomposition of ozone and play a major role in the adsorption, activation and migration of oxygen species, together with O_L to allow the diffusion of surface activated oxygen species, resulting in a better catalytic activity [47].

Text S5. Relationship between adsorption and catalytic ozonation.

The Ag/MnO_2 catalysts were first adsorb N_2 to an equilibrium, and then purging ozone and CH_3SH to start the catalytic ozonation. As shown in Fig. S5, the removal efficiency (74.76%) was much lower than that of catalytic ozonation of CH_3SH directly (98%). This is mainly due to the pre-sorbed N_2 limit the interaction between CH_3SH and Ag/MnO_2, efficiently inactivating the adsorption and catalytic ozonation of CH_3SH. It is reasonable to propose that the pre-adsorbed CH_3SH can efficiently enhance the CH_3SH degradation, vice versa. Moreover, attributed to the high adsorption by Ag/MnO_2 PHMs with 3D structure, it can prolong the retention and contact time of ozone and CH_3SH, thus to make the oxidation more completely.

149

150

151 **Text S6.** Influence of humidity on activity of Ag/MnO_2 PHMSs

152 Generally, humidity is beneficial for the catalytic ozonation [50]. As shown in Figure S4,

153 when the humidity of the inflow CH_3SH was increased from 5% to 67%, the removal

154 efficiency of the optimal 0.3% Ag/MnO_2 PHMSs was further enhanced from 85% to

155 ~100%. It is proposed that the decomposed ozone readily interact with surface OH/H_2O

156 to generate more reactive species like •OH for CH_3SH oxidation. Moreover, the humid

157 air stream can dissolve the accumulated intermediate and release active sites promptly

158 [51].

159

160

Text S7. Reusability and Regeneration of Ag/MnO_2 PHMSs

In industrial applications, the durability of the catalyst is essential for economic and high process efficiency. As shown in Figure S7a, the removal efficiency of CH_3SH decreased to 86% for used Ag/MnO_2 PHMSs in the second run, indicating that Ag/MnO_2 PHMSs show little inactivation. This is mainly ascribed to the surface accumulated intermediates, which could inhibit the adsorption and cover the active sites.

The little inactivation of Ag/MnO_2 PHMSs is presumably due to the surface accumulated intermediates, which could inhibit the adsorption and cover the active sites. Therefore, FTIR was conducted to identify the residual species on the used Ag/MnO_2 PHMSs. As shown in Figure S8, there were new bands occurred at 1164 cm^{-1} (S=O symmetrical stretching vibration) and 1058 cm^{-1} (S-OH stretching vibration), confirming the formation of methanesulfonic acid ($CH_3SO_3^-$) [52]. Meanwhile, other new bands were also observed at 989 cm^{-1} (C-O stretching vibration) and 780 cm^{-1} (S-O stretching vibration), suggesting the C-S bond of CH_3SH was broken and formed into CO_3^{2-} and SO_4^{2-} species [26, 52]. To regenerate the used Ag/MnO_2 PHMSs, ethanol and HCl were utilized to remove the residual S ions. As shown in Figure S6a, after washing by ethanol or HCl, the FTIR peaks of intermediates become weaker and even disappeared, indicating both ethanol and HCl are efficient for the regeneration of Ag/MnO_2 PHMSs. Fortunately, the CH_3SH removal efficiency for the regenerated Ag/MnO_2 PHMSs was recovered from 87.3% to 90.4% (after HCl washing) and 90.6% (after ethanol washing) respectively (Figure S7a)."

The reusability and catalytic stability of Ag/MnO_2 PHMSs were evaluated in the long-term process of successive reusability test (20 cycle runs). Figure S7b shows CH_3SH removal efficiency in 20 cycle runs using Ag/MnO_2 PHMSs. It can be seen that CH_3SH removal efficiency for the regenerated Ag/MnO_2 PHMSs by ethanol washing was 84.7%. This result suggested that Ag/MnO_2 PHMSs displays a relatively stable catalytic

performance for catalytic ozonation of CH_3SH in 20 cycle runs with respect to ethanol-washing regeneration and is a promising catalyst in the practical applications.

Text S8. Conclusion of pathway

On the surface of single atomic Ag/MnO_2 PHMSs, a CH_3SH molecule can be adsorbed by the Ag-SH bond coupling (CH_3S-Ag) and then be nucleophilically attacked by neighboring Ag activated oxygen species. During catalytic ozonation, H_2O first adsorbed to form surface OH groups at the surface sites. Simultaneously, O_3 was interconnected with the catalyst via electrostatic attraction or hydrogen bonding, facilitating electron transfer. In the next phase, H-O and O-O bonds were simultaneously weakened to decompose into $\bullet O_2^-$, $\bullet$OH and $^1O_2$ through a typical chain reaction. With a core intermediate of CH_3S^-, the chemisorption and oxidation are continuously preceded and ultimately mineralize CH_3SH into SO_4^{2-} and CO_3^{2-} by the catalytic ozonation induced ROSs.

Table S1. Specific surface area and degradation rate constants of MnO_2 and Ag/MnO_2 PHMSs.

Catalysts	Ag content	S_{BET}	Total amount of degradation	Degradation rate constant
	wt.%	m^2g^{-1}	10^{-6} mol	10^{-8} mol $g^{-1}s^{-1}$
MnO_2	0	124.13	1.90	3.17
0.1% Ag/MnO_2	0.104	120.87	2.11	3.51
0.2% Ag/MnO_2	0.191	114.45	2.39	3.98
0.3% Ag/MnO_2	0.275	104.11	2.54	4.24
0.5% Ag/MnO_2	0.492	102.95	2.27	3.79
0.75% Ag/MnO_2	0.787	75.29	1.98	3.31
1.0% Ag/MnO_2	1.143	66.17	1.29	2.16

Table S2. Physical parameters, chemical and surface compositions of Mn、O and Ag in Ag/MnO_2 PHMSs.

Sample	Mn^{2+} (%)	Mn^{3+} (%)	Mn^{4+} (%)	O_L (%)	O_{ads} (%)	O_{surf} (%)	Ag^0 (%)	Ag^+ (%)	Surface element molar ratio		
									$Mn^{2+}+Mn^{3+}/Mn^{4+}$	O_L/O_{ads}	Ag^0/Ag^+
MnO_2	6.79	42.13	51.09	62.21	35.23	2.16			0.96	1.78	
Ag/MnO_2	9.96	41.68	48.36	67.94	32.06	0.00	46.75	53.25	1.06	2.12	0.88
Ag/MnO_2 (adsorption)	8.28	42.31	49.41	66.46	33.19	0.35	38.69	61.31	1.02	2.00	0.63
Ag/MnO_2 (ozonation)	5.04	41.83	53.13	60.11	37.56	2.32	40.73	59.27	0.88	1.51	0.69

Table S3. Reduction temperatures and H_2 consumptions of the samples.

Catalysts	Reduction temperatures (℃)[a]			H_2 consumptions (mmol/g) [b]		
	peak 1	peak 2	peak 3	peak 1	peak 2	peak 3
MnO_2	202	311	491	0.79	0.68	3.34
0.3% Ag/MnO_2	114	155	253	1.04	2.83	3.88

[a] Reduction temperatures corresponding to the maximum values of reduction peaks in the H_2-TPR result; [b] H_2 consumptions calculated by reduction peak areas.

Table S4. TOFs for catalytic ozonation of CH_3SH for MnO_2 and Ag/MnO_2 PHMSs.

Catalysts	TOF $\times 10^{-3}$ S^{-1}
MnO_2	0.0437
Ag/MnO_2	2.28

Turnover frequency (TOF) is defined as the number of CH_3SH molecules converted per surface Ag or Mn^{4+} per second.

$$\text{Tureover rate} = \frac{C_{\text{CH3SH}} \times X_{CH3SH} \times \text{Vgas}}{n} [s^{-1}]$$

where C_{CH3SH}: concentration of CH_3SH in gas mixture; X_{CH3SH}: conversion of X_{CH3SH} based on CO_2 formation; Vgas: total molar flow rate; n: mole number of Mn^{4+} ions per gram of Ag/MnO_2 catalyst calculated by H_2—TPR, or mole number of surface Ag of Ag/MnO_2 calculated by Ag dispersion. The Ag dispersions were estimated through a theory of hemisphere models. The calculation method is following.

$$\text{Surface Ag atom number (nsurf)} = \frac{4\pi r^2}{2} \bullet N_A \bullet N_{con}$$

$$\text{Total Ag atom number } (n_{total}) \quad \frac{\rho_{Ag} \bullet (\frac{4}{3}\pi r^3)}{M_{Ag}} \bullet N_A =$$

$$\text{Dispersion (\%)} = \frac{n_{surf}}{n_{total}}$$

where N_A: Avogadro constant; r: the semidiameter of silver nanoparticles; N_{con}: concentration constant of surface silver atoms (N_{con} = 1.15×10^{19} m^{-2}); ρ_{Ag}: density of silver; M_{Ag}: molar mass of silver.

Table S5. Physical parameters, chemical and surface compositions of S in Ag/MnO_2 PHMSs.

Sample	S 2p BE(eV)				Ag-S species (%)	Dimethyl disulfide (%)	Sulfonic acid (%)	Sulfate (%)
	Ag-S species	Dimethyl disulfide	Sulfonic acid	Sulfate				
Ag/MnO_2 (adsorption)	162.61	164.44	168.30	169.52	2.33	29.64	48.29	19.74
Ag/MnO_2 (ozonation)	162.60	164.43	168.19	169.46	1.55	13.74	52.71	32.00

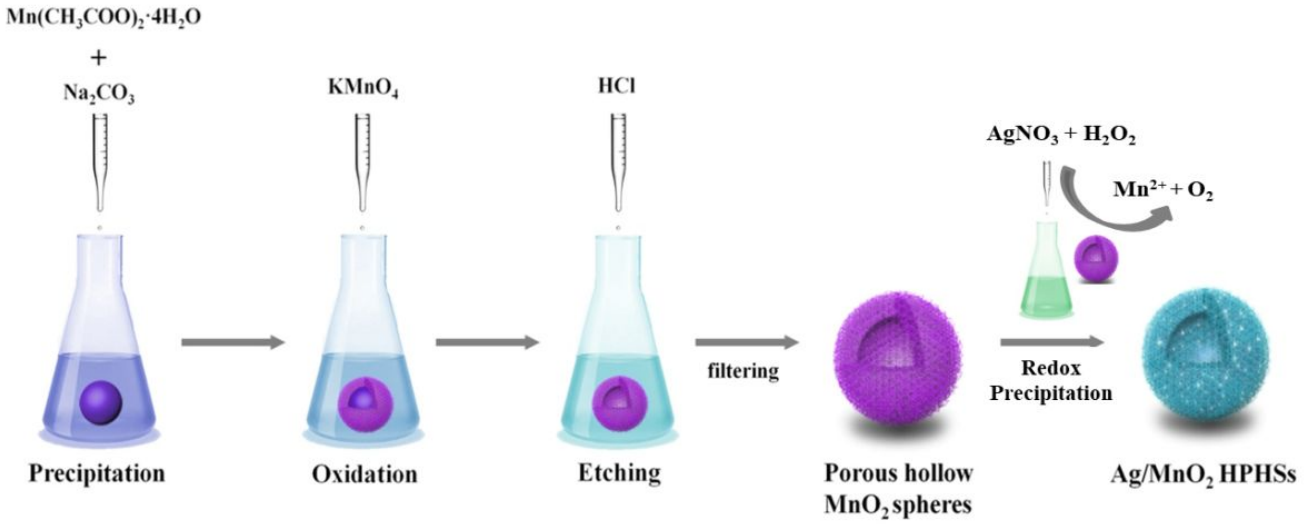

Figure S1. Schematic illustration of the preparation of Ag/MnO_2 PHMSs.

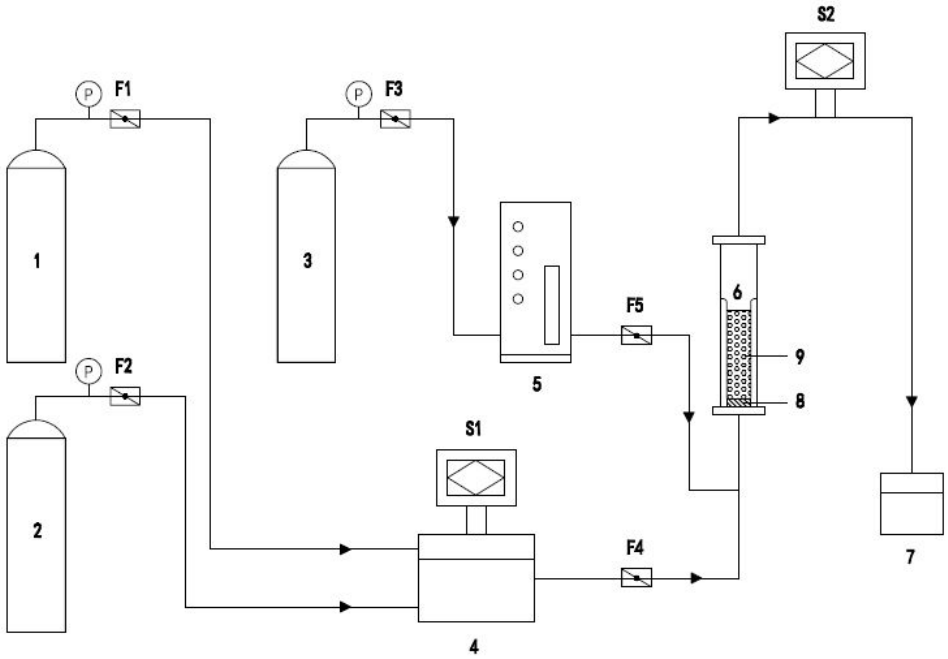

Figure S2. Schematic diagram of system for removal of CH_3SH. 1, CH_3SH gas source; 2, N_2 gas source; 3, O_2 gas source; 4, inlet mixing container; 5, ozone generator; 6, tube reactor; 7, exhaust gas absorption device; 8, sparger; 9, catalysts; F1-F5, gas flow meters; S1-S2, gas sensors of CH_3SH.

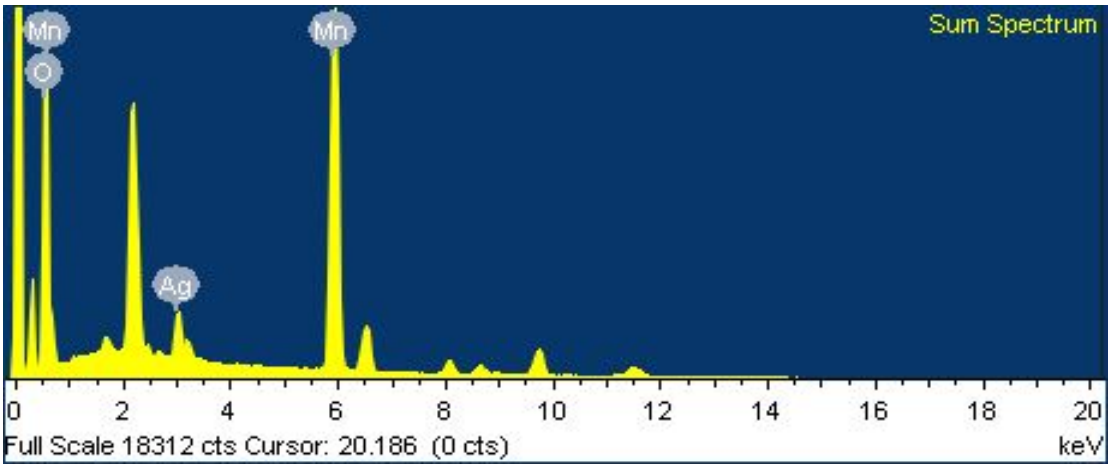

Figure S3. EDS spectra of 0.3% Ag/MnO_2 sample.

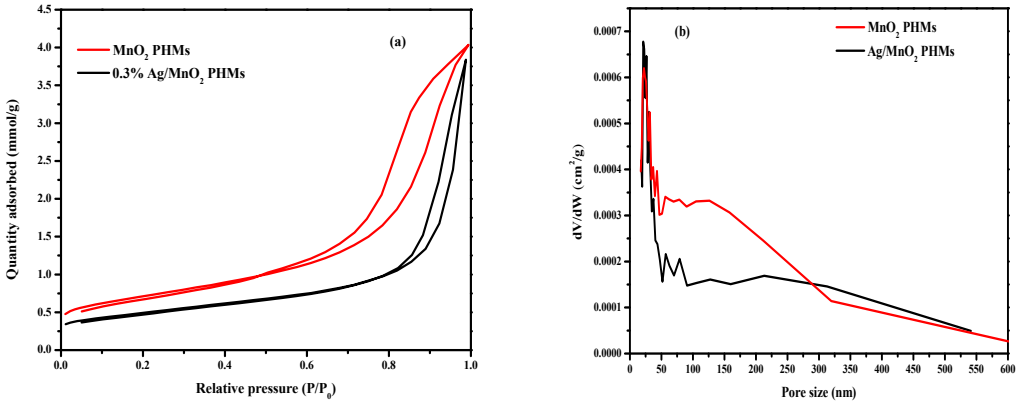

Fig. S4. (a) N_2 adsorption-desorption isotherm and (b) pore size distribution curves of MnO_2 and 0.3%Ag/MnO_2 PHMs.

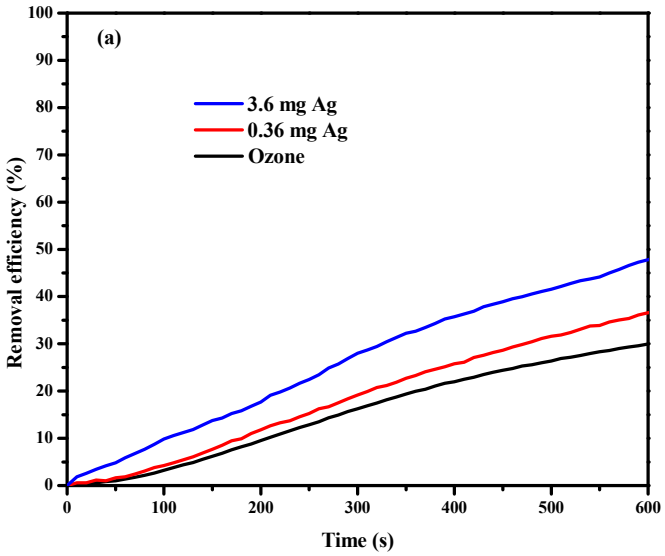

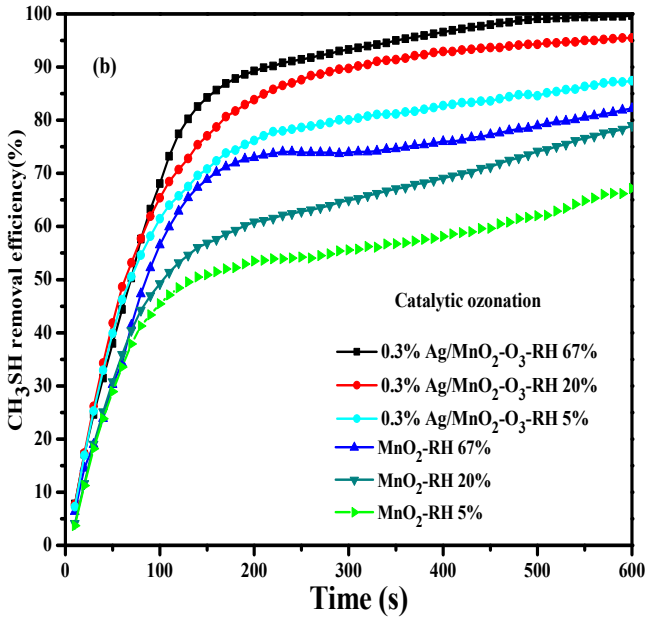

Figure S5. (a) CH_3SH removal efficiency in Ag/O_3 system; (b) Influence of humidity on the activity of 0.3% Ag/MnO_2 PHMSs.

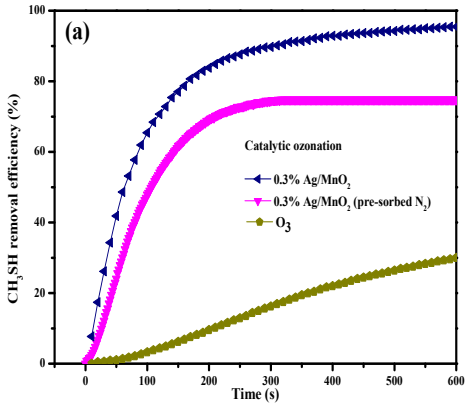

Figure S6. Performances in adsorption and catalytic ozonation of CH_3SH in different system (pre-sorbed N_2).

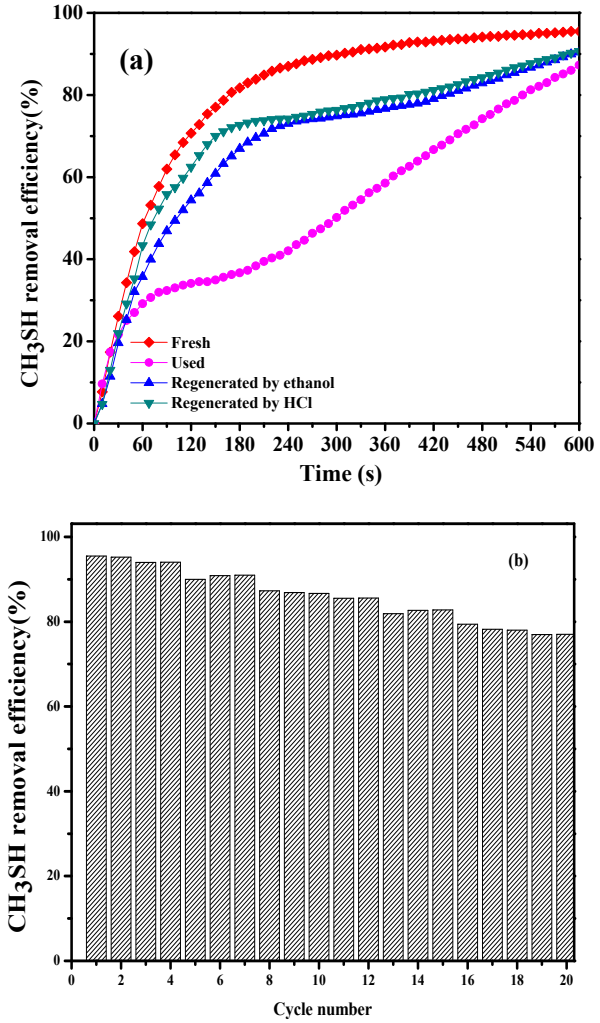

Figure S7. (a) Reusability of 0.3% Ag/MnO_2 PHMSs, and (b) CH_3SH removal efficiency in 20 cycle runs using regenerated 0.3% Ag/MnO_2 PHMSs by ethanol.

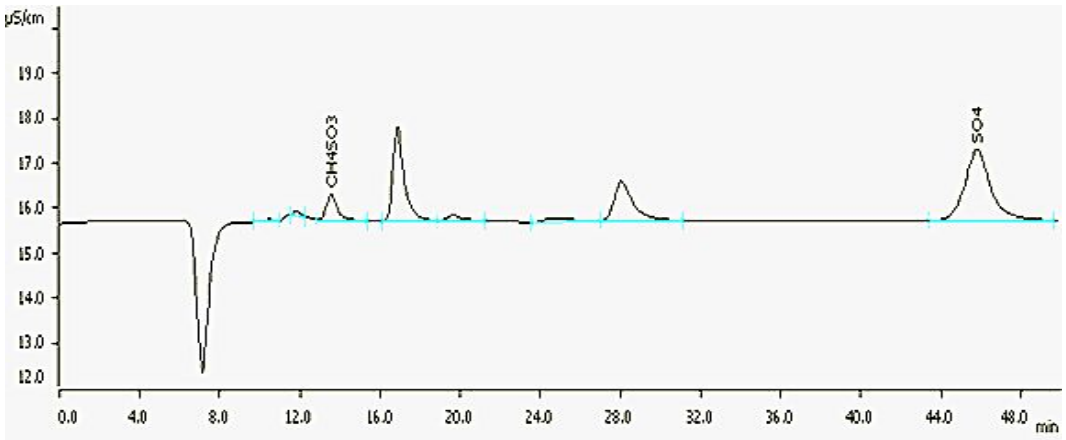

Figure S8. (a) IC analysis of final catalytic products of CH_3SH using Ag/MnO_2 HPMSs; (b) FT-IR spectra of Ag/MnO_2 PHMSs after reaction and regeneration.

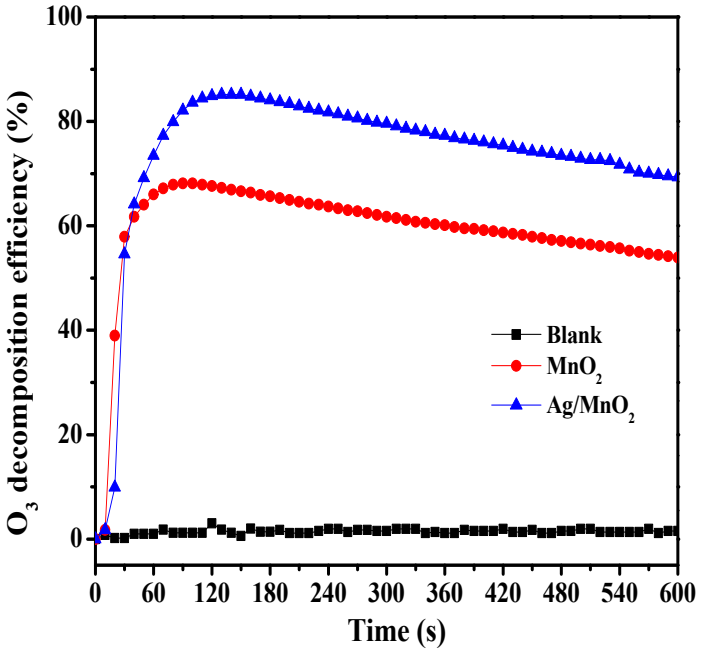

Figure S9. O_3 decomposition by MnO_2 and Ag/MnO_2 PHMSs.